IJL, Issue 2, Vol. 24, 2025
https://doi.org/10.31900/ijl.v24i2.542

Research Article

IRAQI JOURNAL OF LASER

Evaluation of Nd:YAG Laser Spot Welding for Dissimilar Joining of Nickel and Nickel-Coated Copper in Busbar Lithium-Ion Batteries

Vian Jabbar Jumaah[1,2,*], Ziad Aeyad Taha[1], Levent Candan[3], Ersin Kayahan[3]

[1]*Institute of Laser for Postgraduate Studies, University of Baghdad, Baghdad, Iraq*
[2] *Department of Construction and Projects, Al-Nahrain University, Baghdad, Iraq*
[3]*Laser Technologies Research and Application Center (LATARUM), Kocaeli University, 41275, Yeniköy, Kocaeli, Turkey*
*****Email address of the Corresponding author*: vzangana@nahrainuniv.edu.iq

Article history: Received 17 Jun. 2025; Revised 29 Aug. 2025; Accepted 3 Sept. 2025; Published online 15 Dec. 2025

Abstract: This study aims to evaluate the feasibility of using pulsed Nd:YAG laser spot welding to join dissimilar metals consisting of nickel and nickel-plated copper in busbar joints for lithium-ion batteries. The effects of key operating parameters, namely laser energy, pulse repetition rate, and focal position, on the mechanical and structural properties of the weld were examined. The results showed that an energy of 13 joules achieved the highest peak shear force of approximately 273 N with a homogeneous melt zone and limited surface defects, while an energy of 10 joules recorded the highest hardness value (370HV0.300) due to the balance between energy input and cooling rate. It was also found that a repetition rate of 20 Hz and a focal position at 0 mm represent the optimal conditions for obtaining stable mechanical and microstructural properties. Although the results confirm the possibility of obtaining high-quality welds using this technique, full reliability verification requires further analysis through scanning electron microscopy (SEM), phase analysis (EDS/XRD), and fracture pattern studies to determine failure locations. The study also recommends conducting additional experiments to assess long-term performance under various operating conditions such as vibration, temperature fluctuations, and humidity. Thus, this work contributes a scientific basis that can be relied upon to develop more reliable manufacturing processes in modern battery applications.

Keywords: Nd: YAG laser, spot laser welding, Nickel-coated copper, Lithium-ion batteries, mechanical properties.

1. Introduction

Lithium-ion batteries (LIBs) have become the leading technology in energy storage for a wide range of applications, from portable electronic devices to electric vehicles, due to their high energy density, long service life, and excellent efficiency [1]. In such batteries, the electrical connection process between the busbar and the electrode tabs represents a crucial element in ensuring the system's reliability, safety, and long-term performance, as weak or failed weld joints lead to increased electrical resistance, localized hot spots, and possibly premature battery failure. Laser welding techniques have become fundamental methods in modern manufacturing, enabling high speed with limited thermal distortion and minor metallic degradation compared to traditional methods [2,3]. Furthermore, the advancements in laser welding and robotics have provided greater accuracy, flexibility, and higher speed in industrial applications [4]. Pulsed

Nd:YAG laser usage is among the most common choices due to its high efficiency in absorbing reflective metals such as nickel and copper, making it suitable for welding various alloys in battery and electrical applications [5-7].

In contrast, traditional welding methods such as resistance spot welding and ultrasonic welding are less costly and easier to operate, but face significant challenges when used with metals of high thermal conductivity like nickel and nickel-plated copper. Resistance spot welding suffers from electrode wear, poor weld stability, and heat accumulation, whereas ultrasonic welding may lead to weak interfacial bonding or delamination in thin metal sheets. These limitations justify resorting to laser welding despite its relatively higher cost. Nevertheless, welding nickel to nickel-plated copper remains a challenge due to differences in thermal properties, melting points, and reflectivity, which may cause asymmetric weld pools, formation of brittle intermetallic compounds, and development of cracks or porosity in the weld. Numerous studies have addressed dissimilar metal welding in battery applications such as Ni–Al, Cu–Al, and Ni–Cu joints, demonstrating the possibility of improving shear strength, microstructure, and defect control by selecting optimal operating conditions [8–17]. However, research directly focusing on welding nickel to nickel-plated copper remains limited, despite the widespread industrial use of these joints in tab-to-busbar connections in lithium-ion batteries.

Accordingly, this research aims to optimize the parameters of pulsed Nd:YAG laser spot welding for joining nickel to nickel-plated copper, focusing on identifying optimal conditions that achieve high mechanical strength while minimizing surface and structural defects. Through a systematic evaluation of the effects of pulse energy, repetition frequency, and focal distance on shear strength, microhardness distribution, and microstructure, this work seeks to bridge the existing research gap and provide a scientific and practical foundation that can be relied upon in industrial battery manufacturing.

2. Materials

In this study, nickel-coated copper with a thickness of 0.3 mm, sourced from Tata Steel, was utilized as the tab material, along with nickel having a thickness of 0.15 mm. The chemical compositions of these materials are presented in Table 1. The welds were produced in an overlap joint configuration, with the thinner nickel layer positioned on top of the nickel-coated copper layer. The dimensions of the nickel-coated copper and nickel materials were (50 mm × 10 mm × 0.3 mm) and (50 mm × 8 mm × 0.15 mm), respectively with the nickel side facing the laser source. As shown in Figure 1.

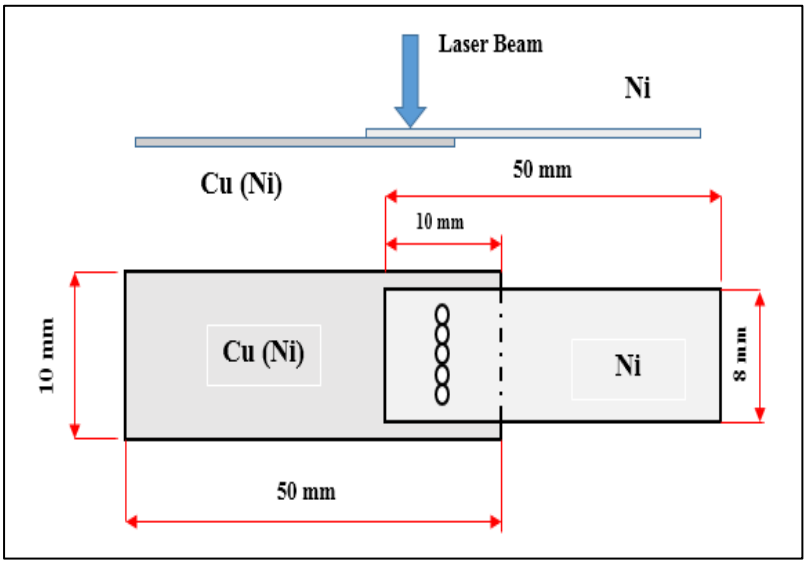

Figure 1: The spot-welding configuration.

Table 1: The chemical composition of Cu (Ni) and Ni materials is based on certifications of Tata Steel and Evek Gmbh, and represents the standard composition as supplied.

Cu (Ni)	Cu	Bi	Pb	Sg	Ni (coated)			
Ni	≥ 99,95 %	≤ 0,0005 %	≤ 0,005 %	≤ 0,030 %	≥ 99,99 %			
	Cu	C	Si	Mn	Ni	Ti	Mg	Fe
	≤0.25	≤ 0.1	≤0.25	≤0.35	≥ 99,2 %	≤0.1	≤0.15	≤0.4

3. Experimental setup and methods

The GSI Lumonics JK760TR Series Laser, an Nd:YAG industrial laser with a wavelength of 1.064 μm, turned into employed for welding. It operates with a mean power of 600 W, peak power of 10 kW, pulse duration of up to 50 ms, and a maximum repetition rate of 500 Hz.

To make sure unique alignment and minimize air gaps, the two plates were firmly secured in a custom clamp. In this setup, a nickel (Ni) plate becomes positioned over a nickel-coated copper (Cu (Ni)) plate, as illustrated in Figure 2. The laser spot at the focus into positioned at the surface of the nickel sheets with a standoff distance of 160 mm and 1.42 mm, the distance between the center of spot and other center and the diameter of the spot of the weld is 0.45mm. No protective shielding gas became used all through the welding process.

Figure 2: schematic of the experimental setup.

A systematic examination of diverse manner parameter units was conducted to gain great stitch welds. Multiple checks have been achieved to perceive the most reliable welding parameters for high-performance joints.

Tables 2 summarize the different parameter sets evaluated, focusing on the outcomes of power, frequency, and focal length with constant pulse duration at 5 ms.

Table 2: Parameters for three groups of welding using different parameters.

Sample No.	Energy (J)	Frequency (Hz)	Focal length (mm)
1	6	20	0
2	8	20	0
3	10	20	0
4	11	20	0
5	13	20	0
6	16	20	0
7	10	10	0
8	10	15	0
9	10	20	0
10	10	30	0
11	10	40	0
12	10	50	0
13	10	20	0
14	10	20	-1
15	10	20	-2
16	10	20	-3
17	10	20	-4
18	10	20	-5

4. Result and Discussion

4.1 Tensile shear test results

The weld joint's mechanical strength under shear loading was evaluated using a tensile shear test. For this evaluation, a uniaxial testing machine (INSTRON, max load capacity: 5 kN) was used. Data for the load displacement curves were obtained by continuously increasing the crosshead speed of the machine until the joint failed, while monitoring the load and displacement.

A. Effect of Energy

The tensile test results (Figure 3) and stress–strain curves (Figure 4) revealed a progressive improvement in weld performance with increasing laser energy. The minimum fracture force at 6 J (41.47 N) indicates a weak bond resulting from insufficient surface fusion (see Figure 5a). Only superficial fusion is observed, which explains the low strength. This low value is consistent with the literature, which suggests that sub-critical energy levels lead to the formation of weak mechanical joints due to inadequate thermal interaction between the surfaces [18].

With an increase in energy to 8 J, a significant improvement in strength is observed, reaching 181.74 N, indicating a notable enhancement in bonding quality (see figure 5 b). Higher energy leads to deeper and more stable fusion. At 10 J, the strength continues to increase to 264.02 N, which signals that the material has entered an effective energy window in which the melting depth balances with thermal conductivity without introducing significant structural defects and at the optimal condition of 13 J, the strength reaches the highest recorded value (273.15 N), indicating a thermally stable process. Studies show that in this range, deep and clean fusion is achieved without the formation of critical defects [19]. (see figure 5 c and e) the cross-sections show relatively deep fusion zones (~159 µm and 215 µm, respectively) corroborating the high mechanical performance.

However, at 11 J, a sudden drop in strength to 153.42 N is recorded despite the increase in energy. This is likely attributed to the initiation of microscopic defects such as porosity or microcracks. Multiple studies, including that of [20], confirm that exceeding a certain energy threshold causes instability in the keyhole regime, leading to gas entrapment and localized collapses that result in porosity formation. (see Figure 5 d) the images reveal signs of microscopic defects, particularly scattered porosity and cracking, which align with the recorded reductions in tensile strength. At 16 J, mechanical performance declines to

231.4 N despite the increase in laser energy. This is due to the increase in thermal porosity and surface shrinkage caused by rapid cooling-phenomena commonly observed in pulsed laser welding when the optimal energy threshold is exceeded [21].

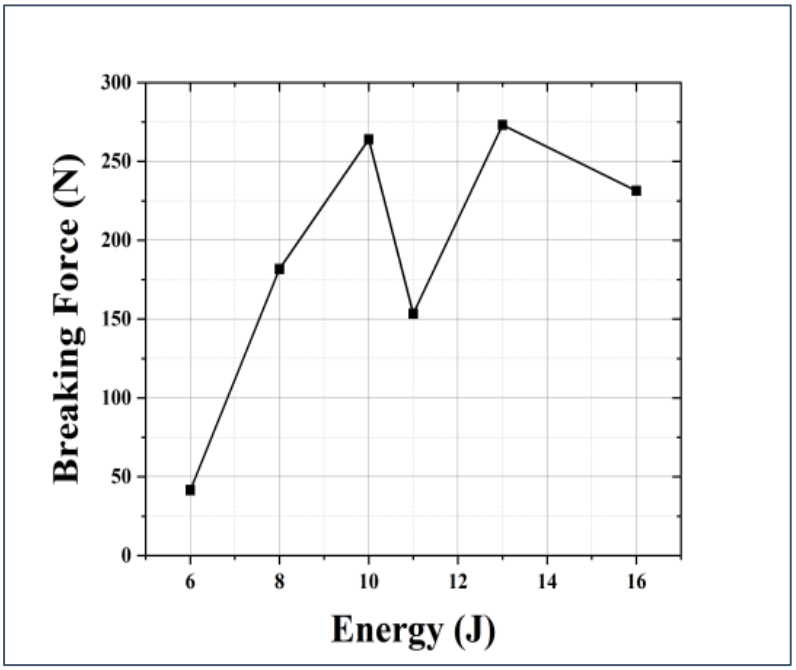

Figure 3: Breaking force versus work energy at constant pulse repetition rate and focal length.

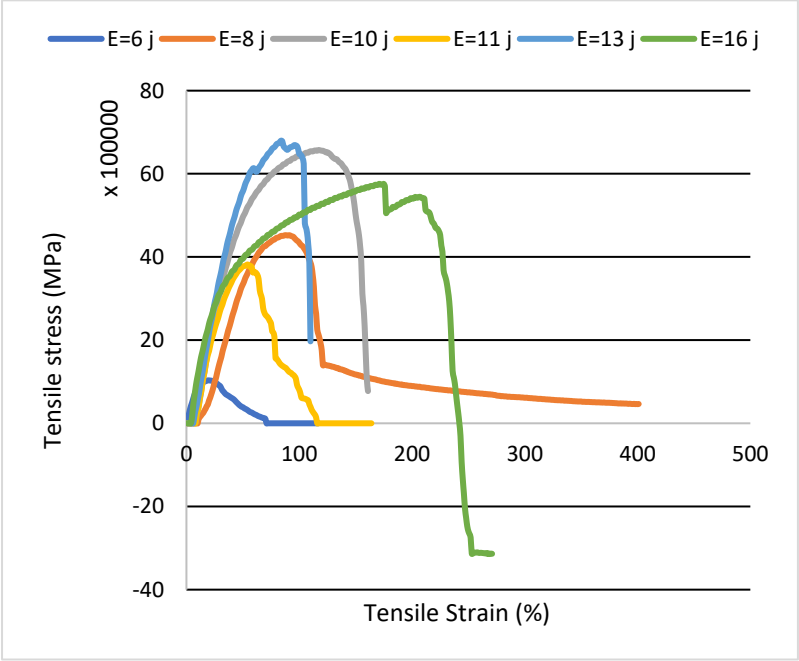

Figure 4: Stress-Strain diagram at different energies.

The stress–strain curve for the 6 J specimen shows a very brittle behavior with rapid failure upon minimal loading. Meanwhile, the curves for 10 J and 13 J display high tensile capacity and extended strain before failure, indicating a strong metallurgical bond capable of effective stress distribution.

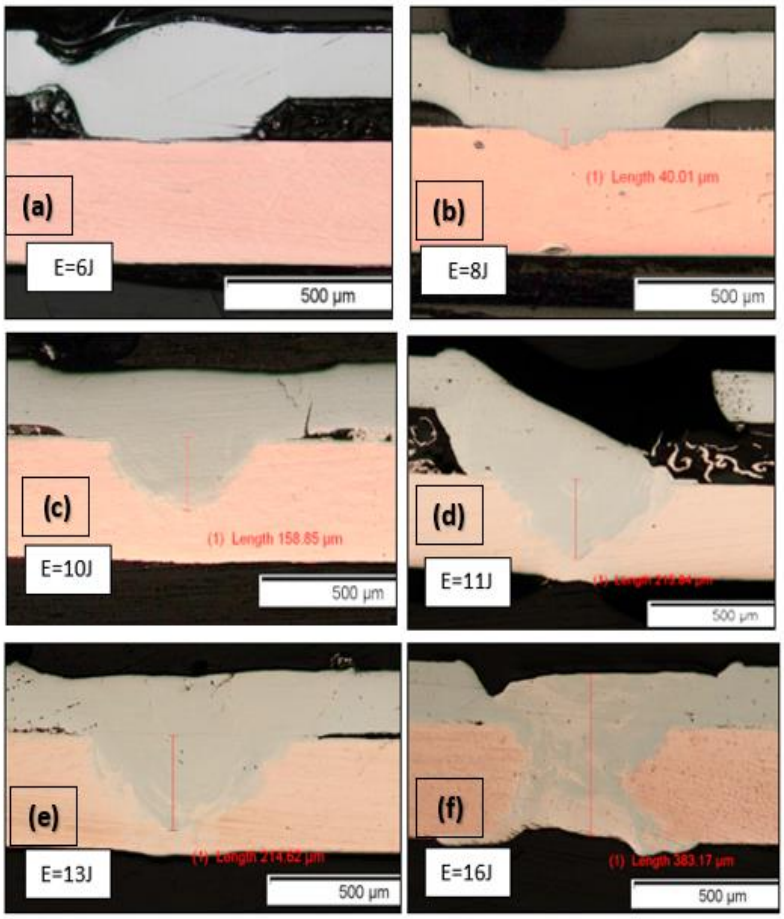

Figure 5: Microscopic images of the weld zones between Ni and Cu (Ni) at different laser energy levels, captured at 5x magnification.

The 11 J curve reveals evident weakness in ductility, reinforcing the assumption of internal defects causing premature failure. Similarly, the 16 J curve shows initially stiff behavior followed by abrupt failure, most likely due to the presence of pores acting as stress concentration points. These results confirm the presence of an "optimal energy window" in the range of 10–13 J, which is necessary to balance adequate penetration and minimize thermal defects, thereby enhancing the mechanical strength of the welded joint.

B. Effect of Pulse Repetition Rate

Figure 6 illustrates the relationship between PRR and fracturing force. At PRR = 10 Hz, the fracture force is at its lowest (70.73 N), indicating a weak bond. Low repetition rates fail to deposit sufficient thermal energy over time to form a stable weld pool, leading to surface-only fusion and likely incomplete bonding [22]. Increasing PRR to 15 Hz raises the force to 172.88 N, suggesting more uniform material fusion due to enhanced heat input and penetration .The peak fracture strength occurs at PRR = 20 Hz, reaching 264.02 N—a clear mechanical optimum. This supports a theory of optimal energy-time balance during welding, creating deep fusion zones without defects such as porosity or cracks [23]. Beyond this point, at PRR = 30 Hz, strength unexpectedly drops to 115.70 N. This decline is attributable to heat saturation in the weld zone,

causing keyhole instability, trapped gas, and micro-porosity [21, 24]. (see figure 7c) PRR = 20 Hz and 30 Hz have deeper weld penetration (≈159μm and 245 μm, respectively) compared to 10 Hz and 50 Hz. However, cracks and heterogeneity at 30 Hz explain its lower strength despite penetration depth.

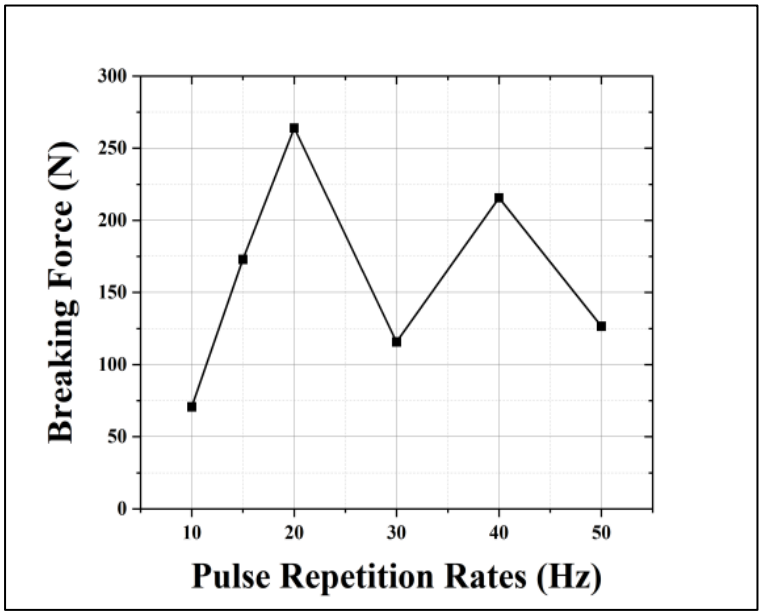

Figure 6: Breaking force versus work pulse repetition rate at constant energy and focal length.

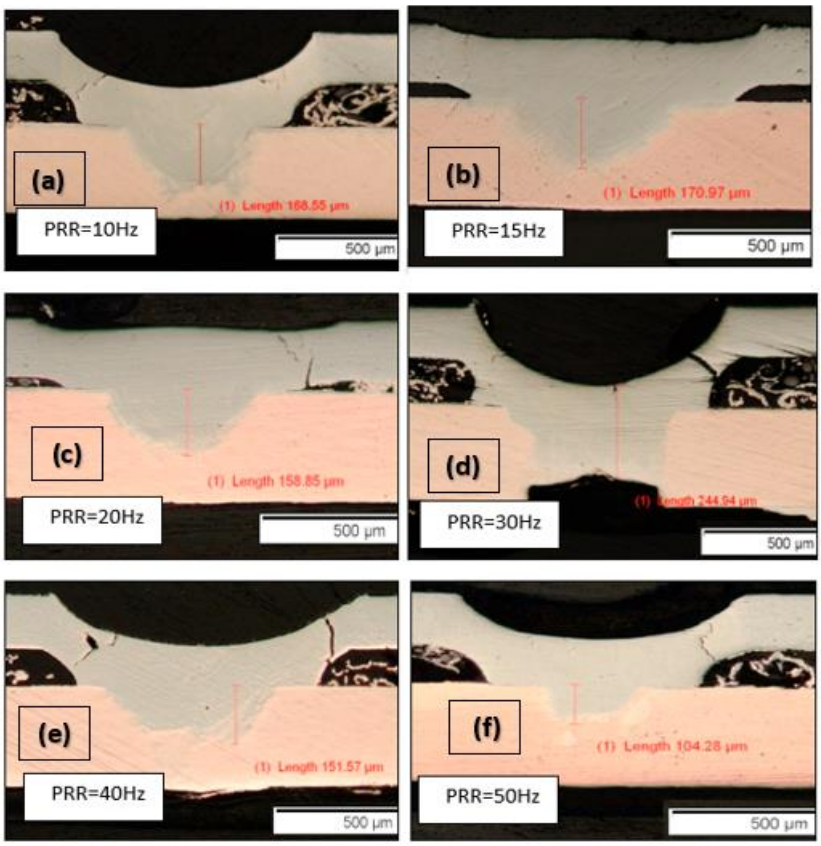

Figure 7: Microscopic images of the weld zones between Ni and Cu (Ni) at different pules repetition rate levels, captured at 5x magnification.

At PRR = 40 Hz, strength partially recovers to 215.60 N—suggesting some regained thermal stability though limited. However, at PRR = 50 Hz, strength falls again to 126.60 N due to unstable heat accumulation and thermally induced defects resulting from rapid thermal cycles (see figure 7 f), penetration is shallow (≈104 µm), confirming inadequate fusion.

This non-linear trend matches the stress–strain curves (Figure 8). PRR = 20 Hz produces the highest maximal stress and strain before fracture, indicative of a robust weld. PRR = 30 Hz and 50 Hz yield brittle behavior and early failure, confirming defect accumulation.

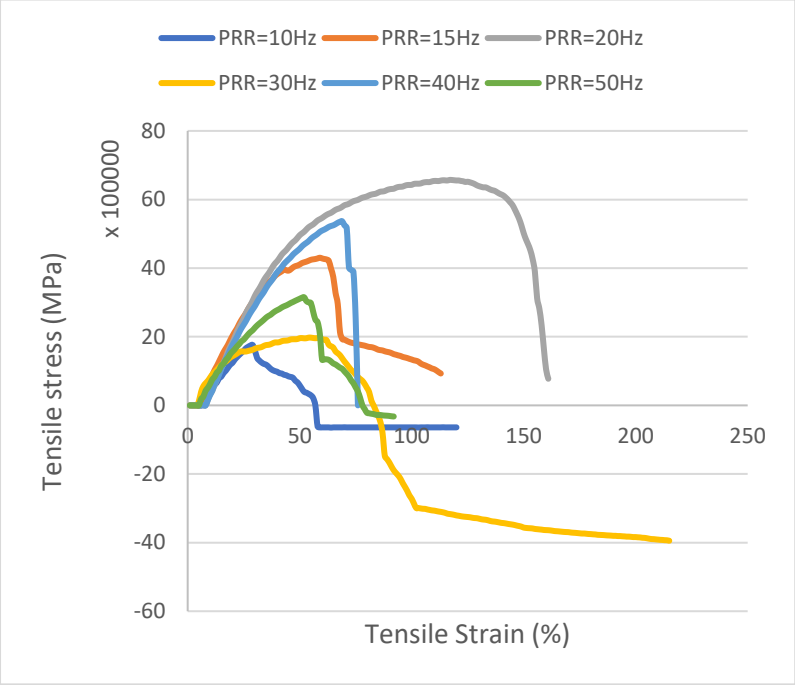

Figure 8: Stress Strain diagram at different pulse repetition rate**.**

Together, these results suggest an optimal PRR near 20 Hz, which balances heat input and dissipation to produce the highest mechanical and structural quality weld. Deviations from this rate in either direction result in defective microstructures and reduced performance.

C. Effect of Focal Length

Based on the data presented in Figure 9, it is evident that laser focal position is a critical factor in determining the mechanical performance of the welded specimen, particularly the maximum fracture force. At zero defocus (0 mm), i.e., when the laser focus is precisely positioned at the interface between the two parts, the highest recorded fracture force (264 N) is achieved. This reflects the formation of a strong metallurgical bond because of complete thermal fusion. The high strength is attributed to the uniform distribution of energy within the keyhole, enabling deep and stable melting followed by gradual solidification, which reduces residual thermal stresses. These findings align with those reported by who emphasized that surface-focused laser positions enhance keyhole stability and minimize disturbances, thereby reducing porosity formation [25].

As the laser focal point shifts downward into the material (negative defocus), the fracture strength decreases progressively: 235 N at –1 mm, 193 N at –2 mm, and finally 108 N at –3 mm. This sharp decline indicates a significant reduction in fusion efficiency due to the decreased power density at the joint interface, as the laser beam spreads over a larger area, lowering the effective energy per unit surface. The resulting

thermal dispersion leads to narrower and shallower fusion zones and increases the likelihood of structural defects, particularly porosity caused by trapped gases or evaporation of high-conductivity materials (see Figure 10). This interpretation is supported by multiple studies [26], who found that defocusing the laser from the optimal position significantly reduced shear strength in fiber laser welding of DP600 dual-phase steel, due to limited transverse thermal conduction and the emergence of fine cracks near the weld seam.

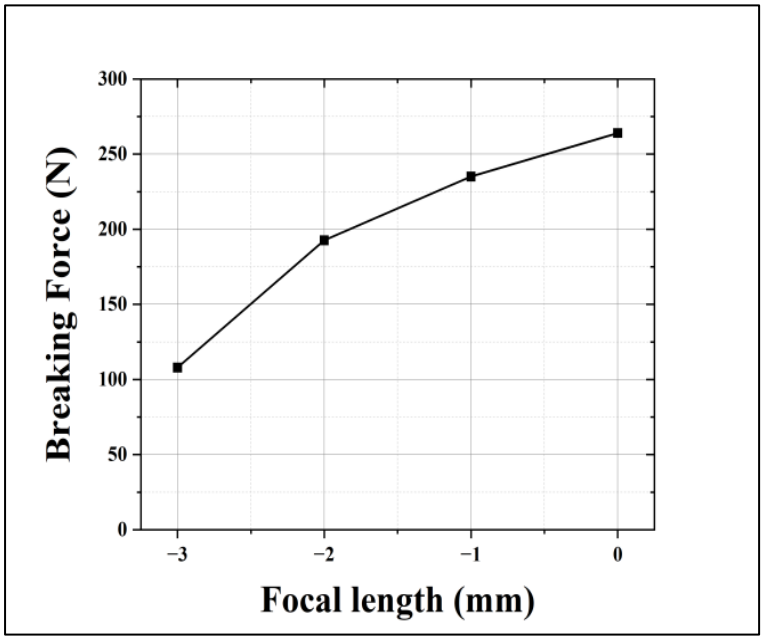

Figure 9: Breaking force versus focal length at constant energy and pulse repetition rate.

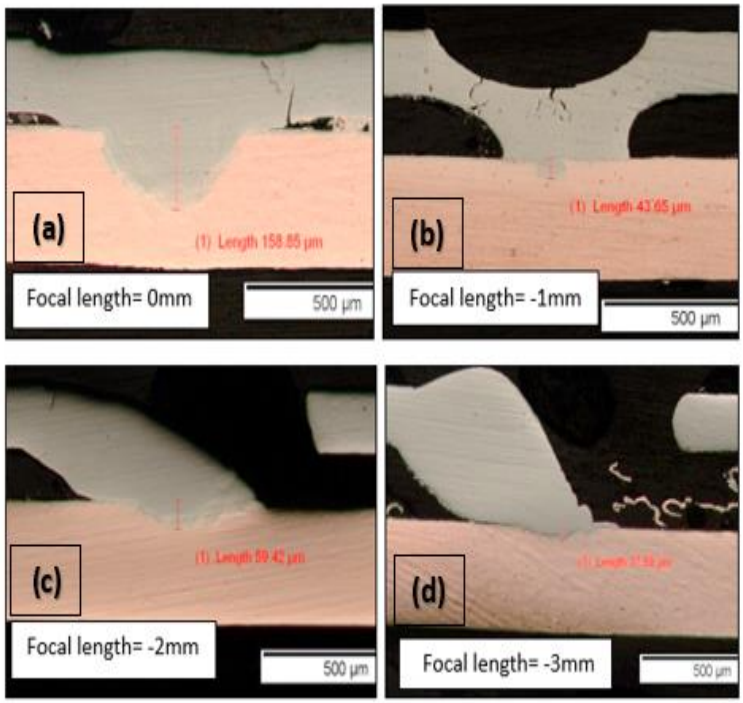

Figure 10: Microscopic images of the weld zones between Ni and Cu (Ni) at different focal length levels, captured at 5x magnification.

The tensile stress–strain curves in Figure 11 reinforce this mechanical analysis by illustrating the deformation behavior of the joint at different focal positions. At 0 mm, the curve exhibits extended strain with a peak stress of about 70 MPa, indicating a strong and ductile joint capable of accommodating significant deformation before failure. At –1 mm, the peak stress drops to around 60 MPa, while still maintaining moderate ductility. This trend continues at –2 mm with a peak of ~50 MPa and reduced elongation, showing early signs of brittle behavior. At –3 mm, the sample fails at ~30 MPa with negligible elongation, reflecting high porosity and microcracking caused by fusion instability. These observations are consistent with the findings who linked reductions in tensile strength and ductility in Cu–Ni alloy welds to porosity distributed along the weld line due to unstable thermal conditions [27].

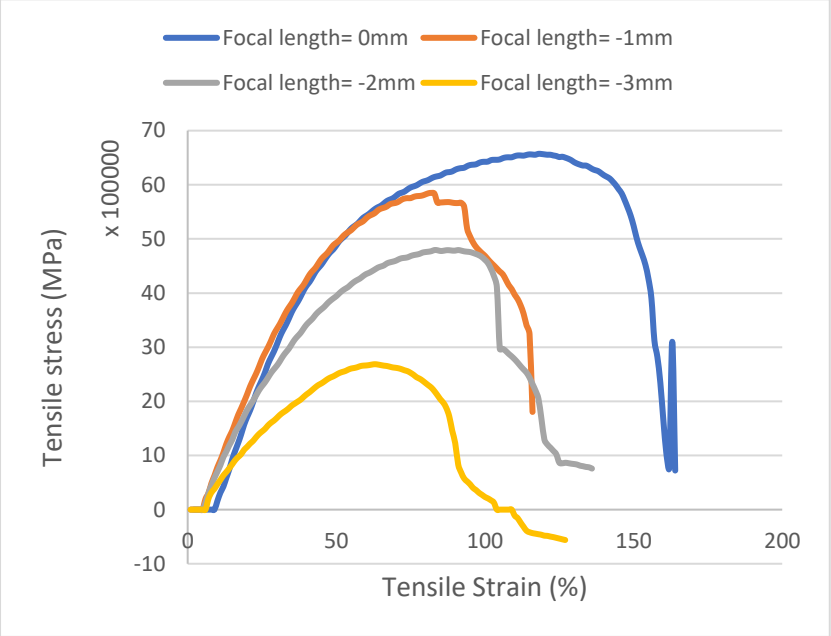

Figure 11: Stress-Strain diagram at different focal lengths**.**

4.2 Micro hardness test results

The hard distribution in the weld cross-section was evaluated using a HARDWAY HVD-1000 AD tester using a 300-gf load. Microhardness testing is a basic mechanical evaluation technique. This is necessary for material characterization following welding and other manufacturing processes. A measurement of resistance to deformation, which provides an important check on the strength and uniformity of a material's internal structure.

A. Effect of Energy

The microhardness graph (Figure 12) clearly shows that hardness is strongly influenced by the applied laser energy. At low energy (6 J), the sample exhibits relatively low hardness at the weld, with a sharp increase at the center line. This suggests a narrow fusion zone and weak metallurgical bonding between the materials, which is also confirmed by the corresponding microscopic image (see Figure 5 a), where the fusion zone appears very limited. Such limited fusion contributes to weaker mechanical properties due to incomplete mixing of Ni and Cu.

At 8 J, the hardness at the weld center improves, reaching over 350 HV. This improvement can be attributed to a greater amount of molten material and an increased cooling rate, resulting in the formation of fine-grained microstructures. This phenomenon has been documented in literature, where rapid solidification leads to grain refinement, thereby enhancing hardness [28].

The corresponding micrograph (see Figure 5 b) supports this, showing a slightly wider fusion zone (~40 µm) than at 6J.

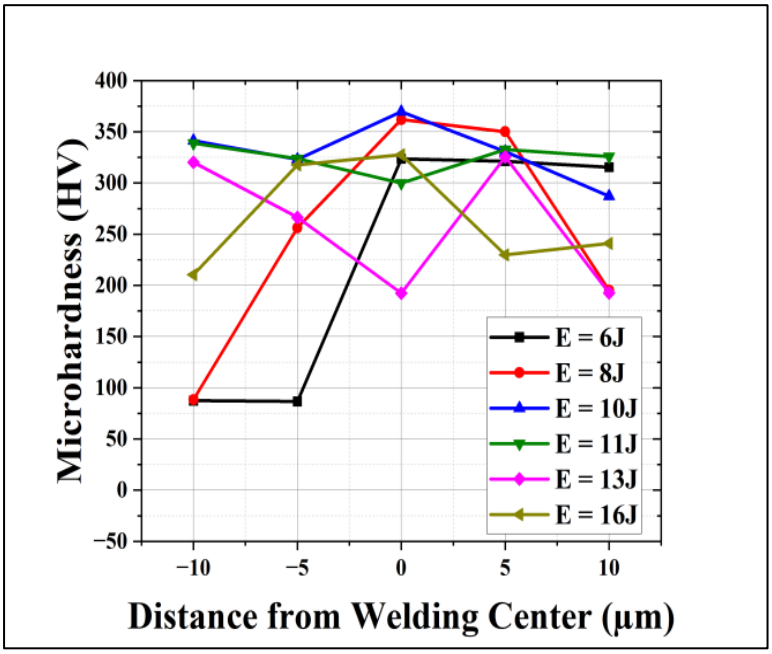

Figure 12: Micro hardness versus distance from welding center for different Energy level.

At 10 J, the highest microhardness (~370 HV) is recorded at the weld center, indicating an optimal balance between energy input and cooling rate, which results in a refined and cohesive weld structure. The microscopic image for this energy level (see Figure 5 c) shows a significantly wider fusion zone (~158.85 µm), which promotes better metallurgical bonding between Ni and Cu, and improves mechanical performance, particularly hardness. As the energy increases to 11 J, the hardness decreases; however, the micrograph reveals an irregular fusion boundary and signs of excessive melting, indicating the onset of thermal instability (see Figure 5 d). This aligns with findings in laser welding studies, where surpassing optimal energy levels leads to microstructural disturbances [21]. The variation in hardness at this stage suggests the emergence of zones with inconsistent mechanical properties.

On 13 J, there is a noticeable drop in hardness (~250 HV) at the weld center, with increased variability across the weld zone. This is likely due to overheating, which promotes the formation of coarse grains because of slower cooling rates. The corresponding microscopic image (see Figure 5 e) shows a clearly expanded fusion zone (~214.62 µm), with visible distortion at the weld interface.

At the highest energy level (16 J), hardness continues to decline to below 350 HV at the weld center. This degradation is attributed to negative effects of excessive heat, including microcracks and porosity caused by localized vaporization or over melting [29]. The micrograph for this condition (see Figure 5 f) reveals an extensively broadened fusion zone (~383.17 µm), with notable microstructural irregularities, which supports the observed decline in microhardness. Based on the graph and microstructural observations, 10 J appears to represent the optimal energy level, providing the best mechanical properties through balanced heat input and rapid solidification. Lower or higher energy levels result in poorer outcomes due to either insufficient fusion or excessive thermal effects, respectively.

B. Effect of Pulse Repetition Rate

Based on Figure 13, it is evident that the microhardness of Ni-Cu(Ni) laser welds is significantly influenced by the pulse repetition rate (PRR). Variations in PRR affect the thermal input, cooling rates, and consequently, the microstructure and presence of defects such as microcracks and porosity. The

microhardness trends correlate with the observed microstructural features, providing insights into the weld quality under different PRR conditions.

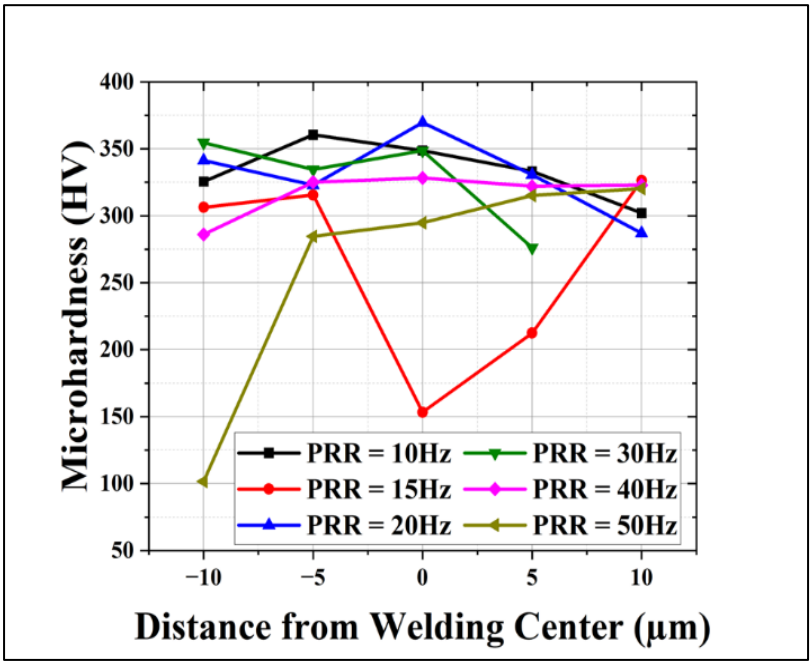

Figure 13: Micro hardness versus distance from welding center for different pulse repetition rate level.

At PRR = 10 Hz this repetition rate, the weld exhibited a high and uniform microhardness (~350 HV) at the weld center. The corresponding microscope (see figure 7 a) shows a homogeneous fusion zone approximately 168.5 μm wide, free from visible cracks or pores. The fine-grained microstructure suggests rapid cooling, leading to improved mechanical properties. This observation aligns with findings who noted that rapid cooling in laser welding promotes fine grain formation, enhancing hardness [28].

An increase in PRR to 15 Hz resulted in a decrease in microhardness at the weld center (~153HV). The micrograph reveals the initiation of micro-porosity within the fusion zone (see figure 7 b), likely due to gas entrapment during solidification. Such porosity can act as stress concentrators, reducing the mechanical strength of the weld. discusses the formation of porosity in laser welding because of rapid solidification trapping gases within the molten pool [21].

At 20 Hz, the weld achieved the highest microhardness (~370 HV) at the center. The fusion zone widened to approximately 158.85 μm (see figure 7c), displaying a fine-grained, defect-free microstructure. This optimal condition suggests a balanced thermal input and cooling rate, facilitating complete fusion and grain refinement. reported similar enhancements in microhardness due to refined microstructures achieved through controlled laser welding parameters [23].

Further increasing the PRR to 30 Hz led to a slight decrease in microhardness (~350 HV) the decrease in hardness at 30 Hz is not necessarily due to visible porosity or cracks, but may result from microscopic changes in the grain structure and cooling rate that depend sensitively on thermal conditions, which affect the hardness without causing obvious micro-defects in the microscopic images (see figure 7 d).

At 40 Hz, the microhardness stabilized at 325 HV. However, the microstructure exhibited increased porosity throughout the fusion zone, particularly near the fusion boundaries. The higher PRR likely led to insufficient time for gas escape, resulting in trapped pores. highlighted that higher laser parameters could increase porosity due to rapid solidification rates [30]. At the highest PRR of 50 Hz, the microhardness decreased to approximately 295 HV, and the fusion zone narrowed to about 104.28 μm (see figure 7f). The micrograph shows a combination of intensified porosity. These defects are attributed to excessive thermal

input leading to overheating, reduced cooling rates, and increased thermal stress. notes that excessive energy input in laser welding can cause such detrimental effects on weld integrity [21].
The analysis indicates that a PRR of 20 Hz offers the optimal balance between thermal input and cooling rate, resulting in the highest microhardness and a defect-free microstructure. Deviations from this optimal PRR, either lower or higher, lead to the formation of microstructural defects such as porosity and microcracks, adversely affecting the mechanical properties of the weld.

C. Effect of Focal Length

Figure 14 shows that the focal length plays a critical role in controlling the efficiency of laser welding for Ni + Cu (Ni) materials, as the mechanical properties and microstructure change significantly depending on the optical focus position. At FL = 0 mm, the highest microhardness (~369.6 HV) was recorded at the weld center, reflecting an ideal concentration of laser energy within the interaction zone. This led to the formation of a fine-grained structure because of a balanced melting and cooling rate (see figure 10a), the microscopic image that showed a clear and homogeneous fusion zone (~158.85 µm).

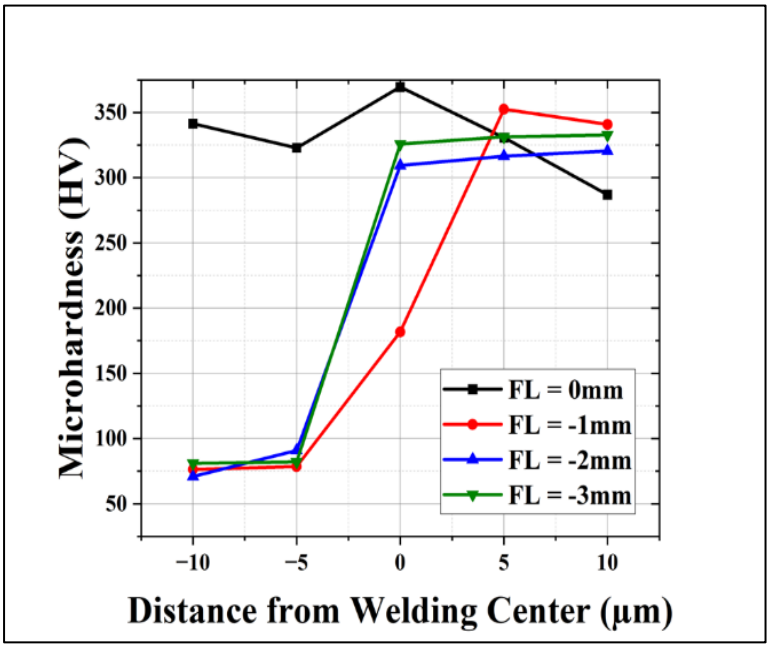

Figure 14: Micro hardness versus distance from welding center for different focal length level.

At FL = -1 mm, the hardness dropped sharply (~181.8 HV), which is attributed to the deviation of the laser beam from the optimal focal point, reducing thermal absorption efficiency and weakening the melting process. (see figure 10 b) The microscopic image for this condition supports the observed decrease in thermal interaction efficiency by showing a narrower fusion zone and a change in the solidification pattern. At FL = -2 mm and FL = -3 mm, a relative improvement in hardness was observed (~309.4 and 325.9 HV, respectively), indicating better distribution of deposited energy on the sample surface. However, the microscopic images revealed a change in the cooling pattern that may be associated with the buildup of internal thermal stresses, potentially leading to the formation of microcracks or microstructural changes at grain boundaries due to the physical interaction between Ni and Cu elements. It is noteworthy that at FL = -4 mm and -5 mm, no visible welding was achieved. This indicates that the laser beam failed to deposit sufficient energy at the interface, which aligns with the physical principle of decreasing power density as the beam moves away from the focal point. This confirms the existence of a critical focal window that must be maintained to ensure effective melting, as supported by previous studies on the influence of optical parameters on laser weld formation [21, 31].

These findings indicate a nonlinear relationship between focal length and welding efficiency, with FL = 0 mm emerging as the most suitable position for achieving stable welds and improved mechanical properties.

5. Conclusions

This study proved that the pulsed Nd:YAG laser welding technique represents a promising option for joining dissimilar metals (Ni/Cu (Ni)) in busbar joints for lithium-ion batteries, provided that operating parameters are precisely controlled. The results showed the following points:

1- Importance of operating parameters: It was concluded that laser energy is the most decisive factor in weld quality. An energy of 13 joules achieved the best mechanical performance (peak shear strength of 273 N) with a homogeneous melt zone and limited surface defects, while an energy of 10 joules achieved the highest hardness value (370 HV). This indicates the existence of an optimal operating window (10–13 joules) that balances melting depth and cooling rate.
2- Effect of pulse repetition rate (PRR): The results showed that 20 Hz is the optimal frequency, providing the highest shear strength and microhardness. Higher frequencies (30–50 Hz) led to thermal accumulation and instability in the weld pool, resulting in porosity and fine cracks, which explains the decline in mechanical performance despite increased penetration depth.
3- Role of focal position: It was found that the 0 mm focus position is optimal for achieving the highest weld strength and homogeneous hardness. Defocusing resulted in weakened metallurgical bonding and increased likelihood of structural defects due to energy dispersion.
4- Microscopic observations: Micrographs showed that the weld microstructure is directly affected by operating parameters; insufficient energy leads to inadequate surface melting areas, while exceeding the optimal energy limit results in porosity and cracks that reduce weld strength and durability.
5- Quality and reliability: Despite achieving high values of strength and hardness, establishing "high quality" welds requires supplementary analyses not included in this work, such as Scanning Electron Microscopy (SEM), elemental analysis (EDS/XRD), and fracture pattern study to determine failure locations. This was pointed out by the reviewer and is considered an essential step in future research.
6- Practical importance and recommendations: The results prove that pulsed Nd:YAG welding can provide reliable joints in battery applications, provided adherence to the optimal parameter window. Additional tests are recommended, including long-term performance under variable operating conditions (such as vibration, temperature fluctuation, and humidity), in addition to in-depth comparisons with previous studies to enhance scientific and practical reliability.

References

[1] M. C. Asirvatham, S. Collins, and I. Masters, "Laser wobble welding of steel to aluminium busbar joints for Li-ion battery packs", Optics and Laser Technology, 151, 108000 (2022).
[2] W. K. Hamoudi, A. K. Hamoudi, and S. A. Salih, "HAZ and melt limits of 3-D CO_2 laser welding", AQI J. Applied Physics, 6, 15-23 (2010).
[3] W. K. Hamoudi, A. K. Hamoudi, and S. A. Salih, "Modeling of 3-D keyhole CO_2 laser welding of steel", AQI J. Applied Physics, (ISSN 1813-2065), (2010).
[4] T. A. Tawfiq, Z. A. Taha, F. I. Hussein, and A. A. Shehab, "Spot welding of dissimilar metals using an automated Nd:YAG laser system", Iraqi J. Laser, Part A, 11, 1-5 (2012).
[5] T. A. Tawfiq, "Parametric optimization of pulsed Nd:YAG laser lap welding of stainless-steel ASTM A240/316L with carbon steel ASTM A570/Gr30", Al-Nahrain J. Engineering Sciences, 20, 27-35 (2017).
[6] A. K. Mahmoud, Z. A. Taha, and A. A. Shehab, "Temperature distribution simulation for pulsed laser spot welding of dissimilar stainless steel AISI 302 to low carbon steel AISI 1008", Advanced Materials Research, 445, 412-417 (2012).
[7] A. A. Shehab, S. K. Sadrnezhaad, A. K. Mahmoud, M. J. Torkamany, A. H. Kokabi, and M. Fakouri Hasanabadi, "Pulsed Nd:YAG laser dissimilar welding of Ti/Al 3105 alloys", Scientia Iranica B, 27, 1982-1994 (2020).
[8] A. Das, D. Li, D. Williams, and D. Greenwood, "Weldability and shear strength feasibility study for automotive electric vehicle battery tab interconnects", J. Brazilian Society of Mechanical Sciences and Engineering, 41, 54 (2019).

[9] N. Kumar, I. Masters, and A. Das, "In-depth evaluation of laser-welded similar and dissimilar material tab-to-busbar electrical interconnects for electric vehicle battery pack", J. Manufacturing Processes, 70, 78-96 (2021).
[10] E. Haddad, J. Helma, A. Olowinsky, and A. Gillner, "Nanosecond pulsed fiber laser as a tool for laser micro welding", Procedia CIRP, 94, 571-576 (2020).
[11] H.-M. Sung, S. Lee, D. Lee, H. Kim, S.-G. Kang, G.-D. Lee, K. Jeong, and N. Han, "Effect of the Ni plating on Al–Cu dissimilar metal laser welded joint", J. Materials Research and Technology, 31, 2473-2483 (2024).
[12] G. Horváth, A. Körmöczi, T. Szörényi, and Z. Geretovszky, "Laser welding and its implementation in the assembly of battery packs in aviation", Int. J. Sustainable Aviation, 6, 51-65 (2020).
[13] F. Yusof, Y. Miyashita, Y. Otsuka, Y. Farazila, W. Hua, and Y. Mutoh, "YAG laser spot welding of PET and metallic materials", (2015).
[14] A. A. Shehab, A. K. Mahmoud, S. K. Sadrnezhaad, M. J. Torkamany, and S. A. Jawad, "Pulsed Nd:YAG laser dissimilar welding of Grade 2 titanium alloy to 3105-O aluminum alloy using AlSi5 filler metal", (unpublished).
[15] A. Mannucci, I. Tomashchuk, V. Vignal, P. Sallamand, and M. Duband, "Parametric study of laser welding of copper to austenitic stainless steel", Procedia CIRP, 74, 450-455 (2018).
[16] G. Horváth, A. Körmöczi, T. Szörényi, and Z. Geretovszky, "Improvement of electrical and mechanical properties of laser welded lap joints via dimensional optimization", Int. J. Advanced Manufacturing Technology, 130, 1843-1854 (2024).
[17] N. Chen, H. Wang, J. Li, V. Liu, and J. Schroth, "Evolution of interfacial microstructure during resistance spot welding of Cu and Al with Ni-P coating", J. Manufacturing Science and Engineering, 144, 041001 (2021). [18] W. Meng, Z.G. Li, and F. Lu, "Porosity formation mechanism and its prevention in laser lap welding for T-joints", J. Mater. Process. Technol., 214, pp.1658–1664 (2014).
[19] Y. Shi, Z. Li, H. Sun, and X. Zhang, "Microstructural characteristics and mechanical properties of pulsed laser lap welded dissimilar joints", Opt. Lasers Eng., 131, 106002 (2020).
[20] B. Zhang and Y. Li, "Defect formation mechanisms in selective laser melting: a review", Chin. J. Mech. Eng., 30(3), pp.515–527 (2017).
[21] S. Katayama, Fundamentals of Laser Welding, Springer (2013).
[22] Y. Liu, Y. Wang, G. Chen, and J. Yang, "Effects of pulse laser parameters on weldability and mechanical performance of dissimilar metal joints", J. Manuf. Process., 35, pp.651–658 (2018).
[23] W. Zhang, H. Li, and D. Sun, "Effect of pulse frequency on microstructure and mechanical properties in pulsed laser welding of Ni–Cu dissimilar metals", Opt. Laser Technol., 139, 106943 (2021).
[24] M. Chludzinski, R.E. dos Santos, C. Churiaque, M. Ortega-Iguña, and J.M. Sánchez-Amaya, "Pulsed laser welding applied to metallic materials—A material approach", Metals, 11(4), 640 (2021).
[25] J. Xu et al., "Keyhole-induced porosity formation during laser welding", J. Mater. Process. Technol., 252, pp.720–727 (2017).
[26] E.S. Atmaca and A. Kurt, "The effects of welding speed and focal length on mechanical characteristic of fiber laser-welded structures of DP600 dual phase steel", GU J. Sci., Part A, 8(1), pp.146–156 (2021).
[27] M.P. Chakravarthy, N. Ramanaiah, and B.S.S. Rao, "Effect of laser welding on mechanical properties of 70/30 Cu-Ni alloy welds", Proc. Inst. Mech. Eng. Part B J. Eng. Manuf., 228(9), pp.1153–1161 (2014).
[28] S. Kou, Welding Metallurgy, 2nd ed., John Wiley & Sons, Hoboken, NJ (2003).
[29] J.R. Davis, ASM Handbook Volume 6: Welding, Brazing, and Soldering, ASM International (1993).
[30] Y. Zhang, H. Zhang, Y. Wu, and X. He, "Influence of laser welding parameters on the microstructure and mechanical properties of dissimilar joints", J. Manuf. Process., 35, pp.580–589 (2018).
[31] W.M. Steen and J. Mazumder, Laser Material Processing, 4th ed., Springer (2010).

تقييم لحام البقعة بالليزر Nd:YAG لربط المعادن غير المتشابهة من النيكل والنحاس المطلي بالنيكل في قضبان التوصيل لبطاريات الليثيوم-أيون

فيان جبار جمعة[1,2]*، زياد اياد طه[1]، ليفنت جاندان[3] ، إيرسن كاياهان[3]

[1]معهد الليزر للدراسات العليا، جامعة بغداد، بغداد، العراق
[2]قسم الاعمار والمشاريع، جامعة النهرين، بغداد، العراق
[3]مركز بحوث وتطبيقات تقنيات الليزر (LATARUM)، جامعة كوجايلي، 41275، ينيكوي، كوجايلي، تركيا

البريد الالكتروني للباحث: vzangana@nahrainuniv.edu.iq

الخلاصة: تهدف هذه الدراسة إلى تقييم جدوى استخدام لحام البقعة بالليزر النبضي نوع Nd:YAG في ربط المعادن غير المتشابهة المكونة من النيكل والنحاس المطلي بالنيكل ضمن وصلات قضبان التوصيل في بطاريات الليثيوم-أيون. تم فحص تأثير معلمات التشغيل الأساسية المتمثلة بطاقة الليزر، معدل تكرار النبضات، والبعد البؤري على الخواص الميكانيكية والبنيوية للحام. أظهرت النتائج أن طاقة 13 جول حققت أعلى قوة قص بلغت حوالي 273 نيوتن مع منطقة انصهار متجانسة وعيوب سطحية محدودة، في حين سجلت طاقة 10 جول أعلى قيمة للصلادة (370HV0.300) نتيجة توازن إدخال الطاقة مع سرعة التبريد. كما تبين أن معدل التكرار 20 هرتز والبعد البؤري عند 0 ملم يمثلان الشرط الأمثل للحصول على خصائص ميكانيكية ومجهرية مستقرة.

ورغم أن النتائج تؤكد إمكانية الحصول على لحامات عالية الجودة باستخدام هذه التقنية، إلا أن إثبات الموثوقية الكاملة يتطلب استكمال التحليل عبر الفحص بالمجهر الإلكتروني الماسح (SEM)، وتحليل الأطوار (EDS/XRD)، ودراسة أنماط الكسر لتحديد مناطق الفشل. كما توصي الدراسة بإجراء تجارب إضافية لتقييم الأداء طويل الأمد تحت ظروف تشغيل متنوعة كالاهتزاز وتغيرات الحرارة والرطوبة. وبذلك يساهم هذا العمل في توفير أساس علمي يمكن الاعتماد عليه لتطوير عمليات تصنيع أكثر موثوقية في تطبيقات البطاريات الحديثة.